

Chiral Majorana Edge Modes and Vortex Majorana Zero Modes in Superconducting Antiferromagnetic Topological Insulator

Beibing Huang,^{1,*} Xiaosen Yang,² Qinfang Zhang,³ and Ning Xu^{1,†}

¹*Department of Physics, Yancheng Institute of Technology, Yancheng, 224051, China*

²*Department of physics, Jiangsu University, Zhenjiang, 212013, China*

³*School of Materials Science and Engineering, Yancheng Institute of Technology, Yancheng 224051, China*

(Dated: November 18, 2021)

The antiferromagnetic topological insulator (AFTI) is topologically protected by the combined time-reversal and translational symmetry \mathcal{T}_c . In this paper we investigate the effects of the s -wave superconducting pairings on the multilayers of AFTI, which breaks \mathcal{T}_c symmetry and can realize quantum anomalous Hall insulator with unit Chern number. For the weakly coupled pairings, the system corresponds to the topological superconductor (TSC) with the Chern number $C = \pm 2$. We answer the following questions whether the local Chern numbers and chiral Majorana edge modes of such a TSC distribute around the surface layers. By the numerical calculations based on a theoretic model of AFTI, we find that when the local Chern numbers are always dominated by the surface layers, the wavefunctions of chiral Majorana edge modes must not localize on the surface layers and show a smooth crossover from spatially occupying all layers to only distributing near the surface layers, similar to the hinge states in a three dimensional second-order topological phases. The latter phase can be distinguished from the former phase by the measurements of the local density of state. In addition we also study the superconducting vortex phase transition in this system and find that the exchange field in the AFTI not only enlarges the phase space of topological vortex phase but also enhances its topological stability. These conclusions will stimulate the investigations on superconducting effects of AFTI and drive the studies on chiral Majorana edge modes and vortex Majorana zero modes into a new era.

INTRODUCTION

The highly effectiveness of quantum computation is rooted in its parallel properties ensured by the superposition principles of quantum mechanism. However the fragileness of quantum systems easily causes random errors in the computational process, which can be overcome by encoding all information into nonlocal qubits (topological quantum computation, TQC) [1, 2]. Majorana fermions [3], realized as the Majorana zero modes in the superconducting vortex [4–13] or the chiral Majorana edge modes [14–17] in the topological superconductors (TSC), can be used to construct topological qubits. However, the computational processes of TQC require braiding the Majorana fermions [2, 18], which is a very difficult task until now for the Majorana zero modes in the superconducting vortex cores. By contrast, the chiral Majorana edge modes can interchange themselves in the transport process and are more easily manipulated [19].

In 2010, Qi etc suggested that chiral Majorana edge modes can be realized as the edge states in the heterostructures of s -wave superconducting proximity to a quantum anomalous Hall insulator (QAHI) [14]. But the experiments in this direction [20–22] arouse much debates about the complicated magnetic disorder effects in the QAHI obtained by magnetically doping the topological insulator [23, 24]. The appearance of the antiferromagnetic topological insulator (AFTI) finds a way out of this dilemma to a large extent [25]. In the AFTI, taking the characteristic Van der Waals layer material MnBi_2Te_4 for example, the magnetic exchanges show

intralayer (interlayer) ferromagnetic (antiferromagnetic) structures with the moments perpendicular to the layer plane, and the topological properties are protected by the combined time-reversal and lattice translational symmetry [26–30]. For an odd (even) number of multilayers, the average moment is nonzero (zero) and the system is an QAHI (axion insulator) with unit (zero) Chern number. The related experiments have observed quantized Hall plateau without the external magnetic field at the high temperature [31–33]. These characters such as stoichiometric purity and Van der Waals structure hint that the slab of AFTI can be used as one of potential candidates to realize the chiral Majorana edge modes.

The multilayers of AFTI have two surfaces and show the gapped surface states. These surface states originate from gapping out the gapless ones of topological insulator and correspond to a half QAHI [34, 35], described by a massive Dirac fermion. Moreover the calculation of local Chern number shows that the contribution to Chern number comes from surface layers, and as one goes deeper, the local Chern number oscillates around zero [36–38]. According to Qi's suggestion [14], once the weakly coupled s -wave pairings are introduced, the multilayers of AFTI with odd number layers become the TSC with Chern number $C = 2$. In this paper, we ask the following two questions. The first one is whether the local Chern numbers of such TSC with $C = 2$ distribute around the surface layers. If the answer is positive, the next question is whether the chiral Majorana edge modes also distribute around the surface layers. By the numerical calculations based on a theoretic model of AFTI, we

find that even if the surface Chern numbers dominate, the wavefunctions of chiral Majorana edge modes must not localize near the surface layers and show a smooth crossover from spatially occupying all layers to only occupying surface layers when some parameters are adjusted. In addition we also study the superconducting vortex phase transition in this system and find that the exchange field in the AFTI not only enlarges the phase space of topological vortex phase but also enhances its topological stability. These conclusions will stimulate the investigations on the superconducting effects of AFTI.

In this paper, we are interested in the TSC with Chern number $C = 2$ realizable in superconducting multilayers of AFTI, which are out of spotlight in contrast to the TSC with $C = 1$. The plan of this paper is as follows. In the section 2, starting from the model of topological insulator, we give the tight-binding model of superconducting multilayer of AFTI by incorporating the antiferromagnetic exchange field in z direction and s -wave on-site intraorbital pairings. In the section 3 we map out the phase diagrams of the system and analyze the distribution of Chern number to exemplify its local properties. We also find that the chemical potential plays an important role in determining available topological phases in our suggested model. The section 4 is devoted to study the wavefunctions of chiral Majorana edge modes. By tracking the evolutions of wavefunctions, we find that the edge modes can continuously evolve into the state only occupying surface layers. We illustrate this crossover from the structure of bulk energy bands. In the section 5, the effects of the antiferromagnetic exchange field on the superconducting vortex phase transition are studied. Finally a brief conclusion is made in the section 6.

MODEL

We start with a four-band model for topological insulators on a cubic lattice with two orbitals and spins per cubic site [39]

$$H_{TI}(k_x, k_y, k_z) = [m + t(\cos k_x + \cos k_y + \cos k_z)]\tau_z + v(\sin k_x \sigma_x + \sin k_y \sigma_y + \sin k_z \sigma_z)\tau_x, \quad (1)$$

where $\sigma_{x,y,z}$ and $\tau_{x,y,z}$ are two sets of Pauli matrices acting on spin and orbital spaces respectively. This Hamiltonian is in the strong topological insulator phase protected by the time-reversal symmetry with $\mathcal{T} = -i\sigma_y\mathcal{K}$ if $|t| < |m| < 3|t|$ and $v \neq 0$, where \mathcal{K} is the complex conjugation operator.

The Hamiltonian of AFTI can be achieved by adding the antiferromagnetic exchange term along z direction into the Hamiltonian (1) [25, 40]. This exchange term breaks the translation symmetry in z direction and magnifies the unit cell of the topological insulator to include

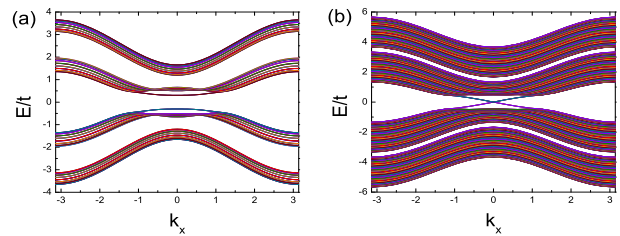


FIG. 1. The excitation spectra in the surface Brillouin zones $k_x k_y$ with $k_y = 0$ (a) and $k_x k_z$ with $k_z = 0$ (b) for the AFTI described by the model (2). In (a) [(b)] the surfaces are ferromagnetic (antiferromagnetic) and breaks (conserves) the combined time-reversal and translational symmetry \mathcal{T}_c , thus the surface states correspond to a gapped (gapless) Dirac fermion. The parameters are $m/t = -2.5$, $v/t = 0.5$, $\Gamma/t = 0.6$.

four orbitals. Choosing the magnetic moment colinear with z direction, AFTI is described by the Hamiltonian

$$H_{AFTI}(k_x, k_y, k_z) = [m + t(\cos k_x + \cos k_y)]\tau_z + \Gamma \varrho_z \sigma_z + \varrho_x [t \cos(k_z/2)\tau_z + v \sin(k_z/2)\sigma_z \tau_x] + v(\sin k_x \sigma_x + \sin k_y \sigma_y)\tau_x, \quad (2)$$

where the Pauli matrices $\varrho_{x,y,z}$ act on the bilayer space induced by antiferromagnetic structure and Γ is the antiferromagnetic exchange field. The model (2) has the combined time-reversal and translational symmetry $\mathcal{T}_c = e^{-ik_z/2}\rho_x\mathcal{T}$ and its topological properties are decided by Z_2 number at $k_z = 0$ plane. We find that as long as the gap from topological insulator is not closed when Γ is increased, the model (2) is an AFTI. In Fig.1(a) and (b), we show the surface states of the model (2), consistent with the our expectations.

In this paper, we consider a multilayer from the AFTI, which is finite length L_z along z direction. At the same time, we also assume that the multilayer is superconducting with s -wave on-site intraorbital pairings. Without loss of generality, we assume all pairings are equal, denoted by Δ . Further introducing Pauli matrices $s_{x,y,z}$ acting on the particle-hole space, our Hamiltonian is

$$H_{SML}(k_x, k_y) = [m + t(\cos k_x + \cos k_y)]s_z \tau_z - \mu s_z + v \sin k_x \sigma_x \tau_x + v \sin k_y s_z \sigma_y \tau_x + \Delta s_y \sigma_y + \frac{t}{2} s_z \tilde{\varrho}_x \tau_z + \frac{v}{2} \tilde{\varrho}_y \sigma_z \tau_x + \Gamma s_z \tilde{\varrho}_z \sigma_z, \quad (3)$$

where we have added the chemical potential μ . The new $L_z \times L_z$ matrices $\tilde{\varrho}_{x,y,z}$ are used to describe the interlayer coupling, which are defined as follows

$$\tilde{\varrho}_{x,y} = \begin{pmatrix} 0 & a & 0 & \dots \\ a^* & 0 & a & \dots \\ 0 & a^* & 0 & \dots \\ \dots & \dots & \dots & \dots \end{pmatrix}, \quad \tilde{\varrho}_z = \begin{pmatrix} 1 & 0 & 0 & \dots \\ 0 & -1 & 0 & \dots \\ 0 & 0 & 1 & \dots \\ \dots & \dots & \dots & \dots \end{pmatrix} \quad (4)$$

with $a = 1$ for $\tilde{\varrho}_x$ and $a = -i$ for $\tilde{\varrho}_y$.

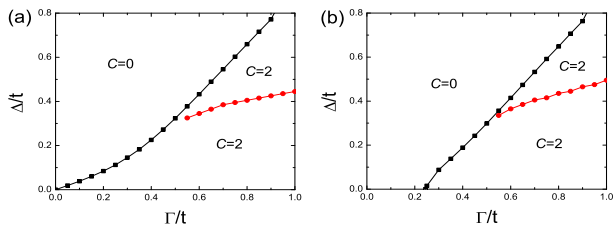


FIG. 2. The phase diagrams for the multilayer model (3) as the function of the antiferromagnetic exchange field Γ and superconducting gap Δ with the chemical potential $\mu/t = 0$ (a) and $\mu/t = 0.1$ (b). The lines with squares separate the normal superconducting phase from the TSC with Chern number $C = 2$; while the lines with circles differentiate two phases in the TSC. These two phases are defined depending on whether the chiral Majorana edge modes only occupy a few layers near the surfaces of the multilayer. The triangle-like regions correspond to such localized phase. It should be noted that in (b) there exists a small phase space not shown for TSC with $C = 1$ between the phases with $C = 2$ and $C = 0$.

The model (3) is our starting point of this paper. We choose the model parameters to ensure that the gap closing of the system happens at $k = 0$. We set $m/t = -2.5$, $v/t = 0.5$.

PHASE DIAGRAM

We construct the phase diagram by tracking the gap closings and the Chern number of the system [41]

$$C = \frac{1}{2\pi} \int dk_x dk_y \text{Tr} \hat{\Omega}_{k,xy} \quad (5)$$

where $\hat{\Omega}_{k,xy}$ are the Berry curvature matrix with

$$\hat{\Omega}_{k,xy}^{nn'} = \nabla_k \times \langle \psi_{nk} | i \nabla_k | \psi_{n'k} \rangle \quad (6)$$

and $|\psi_{nk}\rangle$ is the eigenstates of the occupied bands with eigenvalues E_{nk} in ascending order. We study the Chern number as the function of the antiferromagnetic exchange field Γ and superconducting gap Δ . The phase diagrams for two different chemical potentials are shown in Fig.2.

For $\mu = 0$, the Hamiltonian (3) has an emergent symmetry $\Xi H_{SML}(k_x, k_y) \Xi^{-1} = H_{SML}(k_x, k_y)$ with $\Xi = s_y \sigma_y \tau_y$. This symmetry transforms the particles in an orbital into holes in the other orbital on the same layer but keeps the momentum and spin invariant. Therefore, if $|\psi_{nk}\rangle$ is an eigenstate of $H_{SML}(k_x, k_y)$, $\Xi |\psi_{nk}\rangle$ is also the eigenstate with the same energy. We have numerically checked that these two eigenstates are not linearly correlated. Thus for $\mu = 0$, all energy bands are double degenerate. This result directly influences the available phases in the model (3). Generally the topological phase transition accompanies the gap closings and the dispersion around the phase transition point are gapless Dirac type.

Before and after the phase transition, the Dirac mass is inverted and for every this transition, the Chern number of the system changes ± 1 [42]. Now for $\mu = 0$, the double degeneracy means that the Chern number changes in unit of ± 2 . Since a weakly superconducting coupled QAHI with $C = 1$ realizes a TSC with $C = 2$, thus our system can only show the even Chern number states at $\mu = 0$.

When $\mu \neq 0$, the symmetry Ξ and double degeneracy are broken, thus the Chern number changes in unit of ± 1 and we can observe the TSC with $C = 1$. But in terms of parameters we have chosen, this phase space is very small, so that we do not show this phase region in the phase diagram Fig.2(b). In Fig.2(b), when Γ is small, the system is a normal superconductor. In this region, the normal state is a metal, not a QAHI. With the increase of the exchange field Γ , the gap of the normal state increases. When the gap of the normal state is beyond the chemical potential, the system enters into the topological phase. A finite chemical potential reduces the regions of TSC. This conclusion is consistent with the conventional wisdom.

The Chern number used to differentiate the different phases is defined for the whole multilayer. To study the distribution of Chern number as the function of layer index of multilayer, we need find how different layers contribute to C . This local Chern number C_l for the l th layer can be calculated from the formula [36–38]

$$C_l = \frac{1}{2\pi} \int dk_x dk_y \text{Tr} [\hat{\Omega}_{k,xy} \hat{P}_{k,l}] \quad (7)$$

by inserting a projection $\hat{P}_{k,l}$ onto layer l

$$\hat{P}_{k,l}^{nn'} = \sum_{j \in l} \psi_{nk,j}^* \psi_{n'k,j}, \quad (8)$$

where the summation $j \in l$ is done if the j th component of the eigenfunction ψ_{nk} represents the degree of freedom in layer l . Since $\sum_l \hat{P}_{k,l}^{nn'} = \delta_{n,n'}$, we have $\sum_l C_l = C$. The formalism of C_l was developed for calculating the full surface anomalous Hall conductivity in a multilayer of magnetoelectric insulator.

Below we directly apply this quantity to our case. Fig.3 shows C_l for some different parameters using a 10×10 sampling in the Brillouin zone. In all cases, we find that C_l on the two surface layers approach half of the Chern number of the superconducting multilayer, and as one goes deeper into the interior, C_l oscillates around zero with the average of neighbor layers approaching zero. Therefore the contribution to the whole Chern number comes from a few layers near the surfaces. These results for C_l can be qualitatively understood as follows. We find that the gap of the topological phase in Fig.2 do not close when the hopping in z is adjusted to zero (Fig.3(b)); In addition the spin-orbit coupling in z direction does not influence the gap of the system at the time-reversal

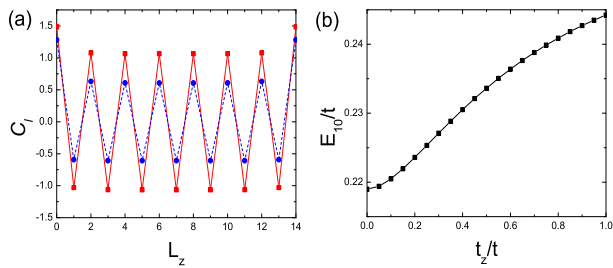


FIG. 3. (a) The local Chern number C_l . With the increase of the superconducting gap, the oscillation of the local Chern number shows decayed amplitude. (b) The evolution of first excitation level E_{1k} at $k = 0$ when the hopping in z direction decreases to zero. The spin-orbit coupling in z direction plays no roles for the gap of the system at the time-reversal invariant momenta. In (a) the parameters for the red solid (blue dashed) line with squares (circles) are $\Gamma/t = 1.0$ and $\Delta/t = 0.02$ ($\Delta/t = 0.65$); In (b) $\Gamma/t = 1.0$, $\Delta/t = 0.6$.

invariant momenta. Therefore from the perspective of topology, it is very appropriate to consider the model (3) adiabatically connected to the model without interlayer couplings. In this limit, every independent layer can be regarded as the TSC with $C = \pm 1$ depending on the sign of the antiferromagnetic exchange field Γ . As a result the Chern numbers of the interior layers average to zero, while surface layers at either end of the multilayer are not completely canceled, realizing a TSC with $C = \pm 1$ at both surfaces.

MAJORANA WAVEFUNCTIONS

In this paper, we are interested in the TSC with $C = 2$. In Fig.3, we have seen that the local Chern number C_l mainly distribute on the surface layers with the averages of the interior layers approaching zero. Now we want to consult that when the Chern number concentrates on the surface layers, whether the chiral Majorana edge modes also concentrates on the surface layers. Below we numerically calculate the wavefunctions of chiral Majorana edge modes to illustrate this question, by assuming an open boundary condition in y direction. Fig.4 shows some characteristic cases for Majorana edge modes.

The normal state of our model is a QAH and always gapped if we decrease the exchange fields Γ on the interior layers to zero but keep them invariant on the two surface layers, thus its chiral edge modes are trapped on the whole side surfaces [34]. On the other hand the TSC with $C = 2$ in the Fig.2 can be continuously connected to the normal state, we naturally expect that when the superconducting gap Δ is small, the chiral Majorana edge modes will occupy all layers of the multilayer, which is consistent with the results in Fig.4(a). While for a big superconducting gap Δ , the wavefunctions are absent from the interior layers and localized near surface layers

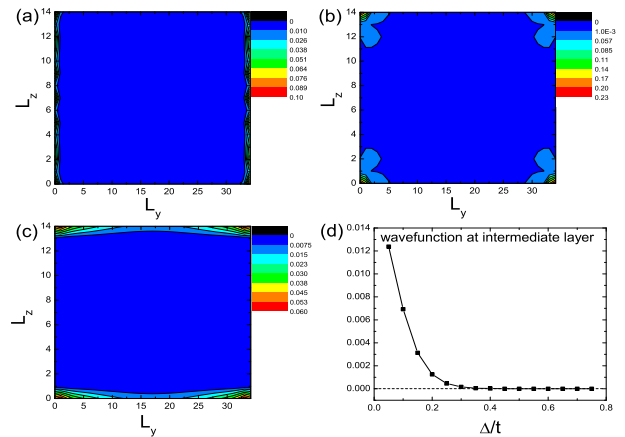


FIG. 4. The evolutions of wavefunctions for the chiral Majorana edge modes as the superconducting gap Δ is adjusted. The parameters are $\Gamma/t = 1.0$ and $\Delta/t = 0.02, 0.65, 0.80$ in (a)-(c).

(Fig.4(b)). This distribution of wavefunctions is similar to the hinge states in a three dimensional second-order topological phases [43–46]. Between these two limits, there is a smooth crossover of wavefunction evolution. From this perspective, we can differentiate two kinds of phases of TSC with $C = 2$. In order to discriminate these two phases, we defined the wavefunctions at intermediate layer of chiral Majorana edge modes equaling to zero as the phase transition point between these two phases. Such behaviors as the function of superconducting gap Δ are shown in Fig.4(d). We have found some phase transition points shown in Fig.2 as the circles for different parameters. For small Γ , the search for the critical point is costly, so we only make some calculations for large Γ . Here we note that such two phases are topologically equivalent with each other, in spite of the differences on the wavefunctions.

The TSC with $C = 2$ will transit into another phase when the superconducting gap is added further. For $\mu = 0$, the system transits into the trivial phase. In this process of phase transition, the chiral Majorana edge modes have the same localization length along the y direction. Increasing the superconducting gap, the localization length gradually increases (Fig.4(c)) and even becomes divergent at the critical point, so that edge modes merge into the bulk states in y direction, leaving a trivial gapped superconductor on the other side of the transition. Similarly for $\mu \neq 0$, there is phase transition to TSC with $C = 1$. The nonzero chemical potential leads to independent evolution of edge modes. At the critical point, one edge mode becomes bulk state while the other is still invariant. But it is worthwhile to note that, the chiral Majorana edge modes always localized near the surface layers in these phase transitions. This property is always invariant.

From the distributions of wavefunctions of chiral Ma-

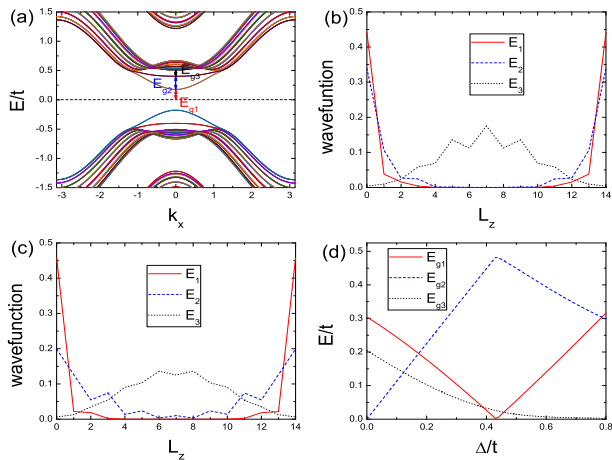


FIG. 5. (a) The excitation spectrum of the multilayer for $k_y = 0$. Three excitation gaps $E_{g1} = E_{10}$, $E_{g2} = E_{20} - E_{10}$, $E_{g3} = E_{30} - E_{20}$ at $k = 0$ are schematically illustrated; (b)-(c) The wavefunctions of three lowest energy levels E_{ik} at $k = 0$ as the function of layer index; (d) The evolutions of three excitation gaps as the function of superconducting pairings. The parameters are $\Delta/t = 0.2$ in (a), $\Delta/t = 0.1$ in (b), $\Delta/t = 0.4$ in (c), $\Gamma/t = 0.6$.

for edge modes, we find that although the Chern number is mainly decided by the surface layers, generally the wavefunctions of edge modes do not only occupy the surface layers. In order to illustrate localization to the surface layers, we observe the evolution of bulk excitation spectrum E_{nk} at $k = 0$, since as stated before we have chosen the model parameters to ensure that the gap closing of the system happens at this point. The excitation spectrum of the multilayer consists of two parts. The first (second) part comes from gapless surface states (gapped bulk states) of topological insulator. When imposed on the staggered magnetic moments and small superconducting pairings, these states still occupied surface layers (bulk) (Fig.5(b)), contributing a large local Chern number to the whole Chern number. Further increasing the superconducting pairings, although the gaps of the system $E_{g1} = E_{10}$ and $E_{g3} = E_{30} - E_{20}$ decrease, the gap $E_{g2} = E_{20} - E_{10}$ gradually increases (Fig.5(d)), not only leading to the mixture of surface energy level E_{2k} into the bulk ones (Fig.5(c)) but also that the low energy properties of the system is only decided to a larger extent by the first excitation level E_{1k} belonging to surface layers. Thus once a boundary is imposed, we expect the chiral Majorana edge modes will also localize near the surface layers. This illustrates our observations on the wavefunctions.

Two kinds of TSC with $C = 2$ have the common bulk properties, however the occupation of the chiral Majorana edge modes near the surface layers should leave the fingerprints on the local low-energy density of state, which can be calculated from the retarded Green func-

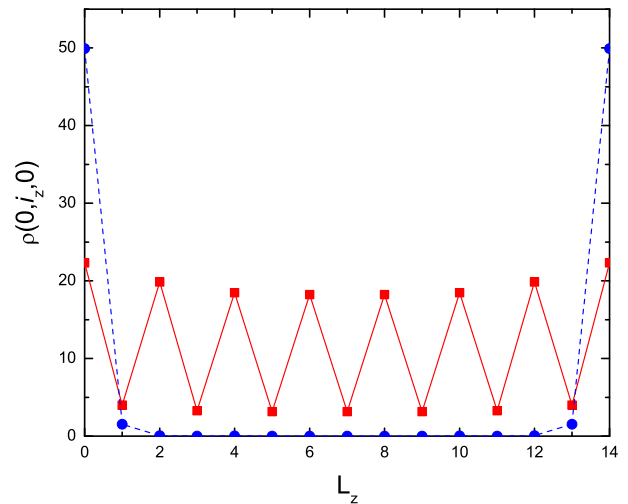


FIG. 6. The local zero-energy density of state $\rho(i_y = 0, i_z, \omega)$ at $\omega = 0$. In order for calculation, we have added a small imaginary part $\delta = 10^{-3}$ to ω . The local zero-energy density of state $\rho(i_y = L_y - 1, i_z, 0)$ shows the same structure. The parameters for the red solid (blue dashed) line with squares (circles) are $\Gamma/t = 1.0$ and $\Delta/t = 0.02$ ($\Delta/t = 0.65$).

tion $\hat{G}_{ret}(k_x, \omega)$ for the system with edges $\rho(i_y, i_z, \omega) = -\sum_{i k_x} \text{Im}[\hat{G}_{ret}^{ii}(k_x, \omega)]$, where the summation for i concerns the all degree of freedom on the lattice site (i_y, i_z) and the label $\text{Im}[\cdot]$ means to take the imaginary part. Fig.6 presents the featured local zero-energy density of state $\rho(i_y = 0, i_z, 0)$ on the side, which has the similar behaviors with the wavefunctions of the chiral Majorana edge modes. Physically $\rho(i_y = 0, i_z, 0)$ can be measured as the zero-bias conductance peak using the scanning tunneling spectroscopy and can be used as the smoking gun to discriminate these two phases experimentally.

VORTEX PHASE TRANSITION

For the topological insulator, a superconducting vortex line will bind two Majorana zero modes, which are localized near the intersections of two surfaces and vortex line when the chemical potential μ is around the charge-neutral point; while tuning μ into the bulk states, a quantum vortex phase transition occurs and two Majorana zero modes disappear [6]. The similar vortex phase transitions have been investigated in superconducting Dirac and Weyl semimetal [49]. In our model, the antiferromagnetic exchange field Γ gap out the surface Dirac point and provides a new knob to manipulate the vortex. Below we will explore the effects of Γ on vortex phase transition.

In order to model a superconducting vortex line in z direction, we assume the superconducting gap Δ in the model (3) acquires the spatial dependence $\Delta_{i_x, i_y} = \Delta_0 \tanh(\sqrt{i_x^2 + i_y^2}/\xi)e^{i\theta}$, where the phase $\theta =$

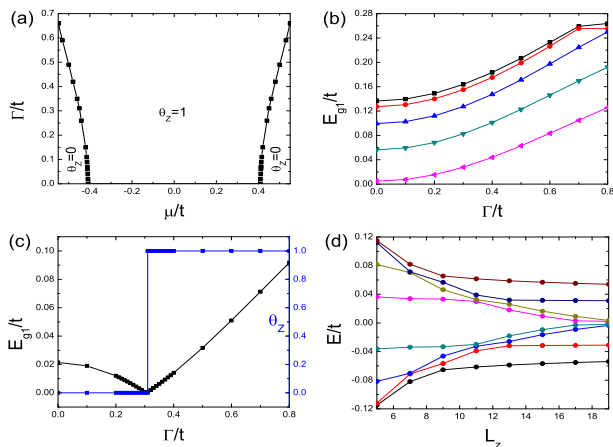


FIG. 7. (a) The phase diagram for one-dimensional vortex line in the superconducting AFTI. The region with Zak phase $\theta_Z = 1$ ($\theta_Z = 0$) is nontrivially (trivially) topological. For $\Gamma = 0$, two critical points of the vortex phase transition are located at $\mu_c/t = \pm 0.41$. (b) The excitation gap E_{g1} as the function of Γ for the different chemical potential. From top to bottom $\mu/t = 0.0, 0.1, 0.2, 0.3, 0.4$ respectively. (c) is the same as (b) except $\mu/t = 0.45$. In this case the excitation shows gap closing and reopening, signifying a vortex phase transition. The change of Zak phase θ_Z is also presented. (d) The scaling behavior of some low-energy eigenvalues for a cubic sample with open boundary condition in all three directions for $\mu/t = 0.1$ and $\Gamma/t = 0.7$. We only show the results for odd number multilayers. Note that for $\mu = 0$, the emergent symmetry Θ leads to the double of Majorana zero modes. In all figures $\Delta_0/t = 0.4$, $\xi = 0.5$.

$\arctan(i_y/i_x)$ reflects the vortex structure and ξ is the superconducting coherence length. We also assume the extreme type II limit to neglect the effect of the magnetic field used to generate the vortices. The vortex line conserves the translational symmetry in the z direction, so that k_z is still a good quantum number and our system can be viewed as a one-dimensional superconductor. However, the complex superconducting gap breaks the combined time-reversal and translational symmetry \mathcal{T}_c and our system is characterized by a well-defined Zak phase θ_z if the energy spectrum is fully gapped [9, 47, 48]. The topological phase diagram from this calculation is shown in Fig.7(a). For $\Gamma = 0$, the system has a nontrivial topological region around the charge-neutral point $\mu = 0$, consistent with others results [6]. With the increase of Γ , the topological region is gradually enlarged. On the other hand, we also find the excitation gap nontrivially increases as the function of Γ for the fixed chemical potential in the topological region (Fig.7(b)), further leading to the robustness of the ground state. These two points signify that the extra controllable knob of the antiferromagnetic exchange field Γ is very advantageous to enhance the topological stability. For the chemical potential beyond the critical points at $\Gamma = 0$ the system shows gap closing, where the sudden jump of Zak phase θ_Z hap-

pens (Fig.7(c)). To further support the results above, we also diagonalize the Hamiltonian for a cubic geometry with open boundary condition in all three directions. In Fig. 7(d), we present some eigenenergies near zero energy for $\mu/t = 0.1$ and $\Gamma/t = 0.7$, their scalings with the system size clearly demonstrate the existence of vortex Majorana zero modes.

For the chemical potential $\mu = 0$, as stated before, there exists an emergent symmetry Ξ . Thus the Hamiltonian can be partitioned into two subspaces related to this symmetry. Considering that the commutation between this symmetry and the particle-hole symmetry, every subspace has also the particle-hole symmetry, thus in every subspace we can also define Zak phase. These two Zak phases is nontrivial for $\mu = 0$. In other words, the emergent symmetry Θ leads to the double of Majorana zero modes at $\mu = 0$. This can be used to illustrate near degeneracy between Majorana zero modes and low energy excitation in Fig.7(d).

CONCLUSIONS

In this paper all calculations have been done for the odd number of multilayers. However the conclusions about the chiral Majorana wavefunctions and vortex phase transition are also applicable to the even number of multilayers. In conclusion we have investigated the effects of the s -wave superconducting pairings on the multilayers of AFTI, which breaks \mathcal{T}_c symmetry and can realize QAH with unit Chern number. For the weakly coupled pairings, the system corresponds to the TSC with the Chern number $C = \pm 2$. By the numerical calculations based on a theoretic model of AFTI, we answered the following questions whether the local Chern numbers and chiral Majorana edge modes of such a TSC distribute around the surface layers. On one hand we find that the local Chern number C_l on the two surface layers approach half of the Chern number of the superconducting multilayer, and as one goes deeper into the bulk, C_l oscillates around zero with the average of neighbor layers approaching zero. Therefore the contribution to the whole Chern number comes from a few layers near the surfaces; On the other hand the wavefunctions of the chiral Majorana edge modes must not localize on the surface layers and show a smooth crossover from spatially occupying all layers to only distributing near the surface layers. These two kinds of topological phases can be distinguished by the measurements of the local density of state. We also discuss the vortex phase transition in this system and find that the antiferromagnetic exchange field not only enlarges the phase space of topological phase but also enhance its the topological stability. Our conclusion will stimulate the investigation on superconducting effects of AFTI and drive the studies on chiral Majorana edge modes into a new era.

ACKNOWLEDGEMENT

We thank Ming Gong for stimulating discussions. B. H. and X. Y. are supported respectively by National Natural Science Foundation of China under Grant No. 11547047 and No. 11504143.

* hbb4236@ycit.edu.cn

† nxu@ycit.cn

- [1] A. Y. Kitaev, *Ann. Phys.* 303, 2 (2003).
- [2] C. Nayak, S. H. Simon, A. Stern, M. Freedman and S. Das Sarma, *Rev. Mod. Phys.* 80, 1083 (2008).
- [3] E. Majorana, *Nuovo Cimento* 5, 171 (1937).
- [4] N. Read and D. Green, *Phys. Rev. B* 61, 10267 (2000).
- [5] L. Fu and C. L. Kane, *Phys. Rev. Lett.* 100, 096407 (2008).
- [6] P. Hosur, P. Ghaemi, R. S. K. Mong and A. Vishwanath, *Phys. Rev. Lett.* 107, 097001 (2011).
- [7] J.-P. Xu, C. Liu, M.-X. Wang, J. Ge, Z.-L. Liu, X. Yang, Y. Chen, Y. Liu, Z.-A. Xu, C.-L. Gao, D. Qian, F.-C. Zhang and J.-F. Jia, *Phys. Rev. Lett.* 112, 217001 (2014).
- [8] H.-H. Sun, K.-W. Zhang, L.-H. Hu, C. Li, G.-Y. Wang, H.-Y. Ma, Z.-A. Xu, C.-L. Gao, D.-D. Guan, Y.-Y. Li, C. Liu, D. Qian, Y. Zhou, L. Fu, S.-C. Li, F.-C. Zhang and J.-F. Jia, *Phys. Rev. Lett.* 116, 257003 (2016).
- [9] G. Xu, B. Lian, P. Tang, X.-L. Qi and S.-C. Zhang, *Phys. Rev. Lett.* 117, 047001 (2016).
- [10] P. Zhang, K. Yaji, T. Hashimoto, Y. Ota, T. Kondo, K. Okazaki, Z. Wang, J. Wen, G. D. Gu, H. Ding and S. Shin, *Science* 360, 182 (2018).
- [11] D. Wang, L. Kong, P. Fan, H. Chen, S. Zhu, W. Liu, L. Cao, Y. Sun, S. Du, J. Schneeloch, R. Zhong, G. Gu, L. Fu, H. Ding and H.-J. Gao, *Science* 362, 333 (2018).
- [12] Q. Liu, C. Chen, T. Zhang, R. Peng, Y.-J. Yan, C.-H.-P. Wen, X. Lou, Y.-L. Huang, J.-P. Tian, X.-L. Dong, G.-W. Wang, W.-C. Bao, Q.-H. Wang, Z.-P. Yin, Z.-X. Zhao and D.-L. Feng, *Phys. Rev. X* 8, 041056 (2018).
- [13] C. Chen, Q. Liu, T.-Z. Zhang, D. Li, P.-P. Shen, X.-L. Dong, Z.-X. Zhao, T. Zhang and D.-L. Feng, *Chin. Phys. Lett.* 36, 057403 (2019).
- [14] X.-L. Qi, T. L. Hughes, S.-C. Zhang, *Phys. Rev. B* 82, 184516 (2010).
- [15] J. Wang, Q. Zhou, B. Lian and S.-C. Zhang, *Phys. Rev. B* 92, 064520 (2015).
- [16] J. D. Sau, R. M. Lutchyn, S. Tewari and S. Das Sarma, *Phys. Rev. Lett.* 104, 040502 (2010).
- [17] J. Alicea, *Phys. Rev. B* 81, 125318 (2010).
- [18] D. A. Ivanov, *Phys. Rev. Lett.* 86, 268 (2001).
- [19] B. Lian, X.-Q. Sun, A. Vaezi, X.-L. Qi and S.-C. Zhang, *Proc. Natl. Acad. Sci.* 115, 10938 (2018).
- [20] Q. L. He, L. Pan, A. L. Stern, E. C. Burks, X. Che, G. Yin, J. Wang, B. Lian, Q. Zhou, E. S. Choi, K. Murata, X. Kou, Z. Chen, T. Nie, Q. Shao, Y. Fan, S.-C. Zhang, K. Liu, J. Xia and K. L. Wang, *Science* 357, 294 (2017).
- [21] J. Shen, J. Lyu, J. Z. Gao, Y.-M. Xie, C.-Z. Chen, C. Cho, O. Atanov, Z. Chen, K. Liu, Y. J. Hu, K. Y. Yip, S. K. Goh, Q. L. He, L. Pan, K. L. Wang, K. T. Law and R. Lortz, *Proc. Natl. Acad. Sci.* 117, 238 (2020).
- [22] M. Kayyalha, D. Xiao, R. Zhang, J. Shin, J. Jiang, F. Wang, Y.-F. Zhao, R. Xiao, L. Zhang, K. M. Fijalkowski, P. Mandal, M. Winnerlein, C. Gould, Q. Li, L. Molenkamp, M. H. W. Chan, N. Samarth and C.-Z. Chang, *Science* 367, 64 (2020).
- [23] W. Ji and X.-G. Wen, *Phys. Rev. Lett.* 120, 107002 (2018).
- [24] Y. Huang, F. Setiawan and J. D. Sau, *Phys. Rev. B* 97, 100501 (2018).
- [25] R. S. K. Mong, A. M. Essin and J. E. Moore, *Phys. Rev. B* 81, 245209 (2010).
- [26] M. M. Otrokov et al., *Nature (London)* 576, 416 (2019).
- [27] M. M. Otrokov, I. P. Rusinov, M. Blanco-Rey, M. Hoffmann, A. Y. Vyazovskaya, S. V. Eremin, A. Ernst, P. M. Echenique, A. Arnau and E. V. Chulkov, *Phys. Rev. Lett.* 122, 107202 (2019).
- [28] Y. Gong, J. Guo, J. Li, K. Zhu, M. Liao, X. Liu, Q. Zhang, L. Gu, L. Tang, X. Feng, D. Zhang, W. Li, C. Song, L. Wang, P. Yu, X. Chen, Y. Wang, H. Yao, W. Duan, Y. Xu, S.-C. Zhang, X. Ma, Q.-K. Xue and K. He, *Chin. Phys. Lett.* 36, 076801 (2019).
- [29] D. Zhang, M. Shi, T. Zhu, D. Xing, H. Zhang and J. Wang, *Phys. Rev. Lett.* 122, 206401 (2019).
- [30] J. Li, Y. Li, S. Du, Z. Wang, B.-L. Gu, S.-C. Zhang, K. He, W. Duan and Y. Xu, *Sci. Adv.* 5, eaaw5685 (2019).
- [31] Y. Deng, Y. Yu, M. Z. Shi, Z. Guo, Z. Xu, J. Wang, X. H. Chen and Y. Zhang, *Science* 367, 895 (2020).
- [32] C. Liu, Y. Wang, H. Li, Y. Wu, Y. Li, J. Li, K. He, Y. Xu, J. Zhang and Y. Wang, *Nat. Mater.* 19, 522 (2020).
- [33] J. Ge, Y. Liu, J. Li, H. Li, T. Luo, Y. Wu, Y. Xu and J. Wang, *Natl Sci. Rev.* 7, 1280 (2020).
- [34] X.-L. Qi, T. L. Hughes and S.-C. Zhang, *Phys. Rev. B* 78, 195424 (2008).
- [35] L. Fu and C. L. Kane, *Phys. Rev. B* 76, 045302 (2007).
- [36] A. M. Essin, J. E. Moore and D. Vanderbilt, *Phys. Rev. Lett.* 102, 146805 (2009).
- [37] T. Rauch, T. Olsen, D. Vanderbilt and I. Souza, *Phys. Rev. B* 98, 115108 (2018).
- [38] N. Varnavaal and D. Vanderbilt, *Phys. Rev. B* 98, 245117 (2018).
- [39] P. Hosur, S. Ryu and A. Vishwanath, *Phys. Rev. B* 81, 045120 (2010).
- [40] P. Yang and Y. Xu, *Phys. Rev. B* 99, 195431 (2019).
- [41] T. Fukui, Y. Hatsugai and H. Suzuki, *J. Phys. Soc. Japan* 74, 1674 (2005).
- [42] J. Bellissard, arXiv:cond-mat/9504030.
- [43] W. A. Benalcazar, B. A. Bernevig and T. L. Hughes, *Science* 357, 61 (2017).
- [44] W. A. Benalcazar, B. A. Bernevig and T. L. Hughes, *Phys. Rev. B* 96, 245115 (2017).
- [45] F. Schindler, A. M. Cook, M. G. Vergniory, Z. Wang, S. S. P. Parkin, B. A. Bernevig and T. Neupert, *Sci. Adv.* 4, eaat0346 (2018).
- [46] Z. Song, Z. Fang and C. Fang, *Phys. Rev. Lett.* 119, 246402 (2017).
- [47] Y. Hatsugai, *J. Phys. Soc. Jpn.* 75, 123601 (2006).
- [48] J. C. Budich and E. Ardonne, *Phys. Rev. B* 88, 075419 (2013).
- [49] Z. Yan, Z. Wu and W. Huang, *Phys. Rev. Lett.* 124, 257001 (2020).